The Journal of Chemical Physics

Does the Adam-Gibbs relation hold in simulated supercooled liquids?

Cite as: J. Chem. Phys. **151**, 084504 (2019); https://doi.org/10.1063/1.5113477
Submitted: 04 June 2019 . Accepted: 04 August 2019 . Published Online: 28 August 2019

Misaki Ozawa, Camille Scalliet, Andrea Ninarello, and Ludovic Berthier

The Journal of Chemical Physics ARTICLE scitation.org/journal/jcp

Does the Adam-Gibbs relation hold in simulated supercooled liquids?

Cite as: J. Chem. Phys. 151, 084504 (2019); doi: 10.1063/1.5113477
Submitted: 4 June 2019 • Accepted: 4 August 2019 •
Published Online: 28 August 2019

Misaki Ozawa,[1] Camille Scalliet,[1] Andrea Ninarello,[2] and Ludovic Berthier[1,a)]

AFFILIATIONS

[1] Laboratoire Charles Coulomb (L2C), Université de Montpellier, CNRS, Montpellier, France
[2] CNR-ISC Uos Sapienza, Piazzale A. Moro 2, IT-00185 Roma, Italy

[a)] ludovic.berthier@umontpellier.fr

ABSTRACT

We perform stringent tests of thermodynamic theories of the glass transition over the experimentally relevant temperature regime for several simulated glass-formers. The swap Monte Carlo algorithm is used to estimate the configurational entropy and static point-to-set lengthscale, and careful extrapolations are used for the relaxation times. We first quantify the relation between configurational entropy and the point-to-set lengthscale in two and three dimensions. We then show that the Adam-Gibbs relation is generally violated in simulated models for the experimentally relevant time window. Collecting experimental data for several supercooled molecular liquids, we show that the same trends are observed experimentally. Deviations from the Adam-Gibbs relation remain compatible with random first order transition theory and may account for the reported discrepancies between Kauzmann and Vogel-Fulcher-Tammann temperatures. Alternatively, they may also indicate that even near T_g thermodynamics is not the only driving force for slow dynamics.

I. INTRODUCTION

Since its first derivation in 1965,[1] the Adam-Gibbs relation has played a central role in glass transition studies[2] since it is at the core of thermodynamic approaches to the glass problem.[1–9] The Adam-Gibbs relation captures in a simple mathematical form the physical idea that the decrease in the configurational entropy $S_{\rm conf}$ controls the growth of the relaxation time τ_α as the experimental glass transition temperature T_g is approached,

$$\log(\tau_\alpha/\tau_0) \propto \frac{1}{TS_{\rm conf}}, \tag{1}$$

where τ_0 is a microscopic time scale. Testing the Adam-Gibbs relation has almost become synonymous to testing the thermodynamic nature of glass formation.[10–13]

Since computational methods have become available in the early 2000s to measure the configurational entropy in numerical simulations,[14–16] the Adam-Gibbs relation has been tested in a large number of studies using many different models of glass-forming materials.[12,17–24] Importantly, these simulations are all restricted to a high temperature regime (typically above the mode-coupling crossover temperature $T_{\rm mct}$[25]) that barely overlaps with the corresponding experimental studies. In addition, simulations typically cover a dynamic window of at most 3–4 decades, much narrower than in experimental studies. Despite these caveats, the general consensus is that the Adam-Gibbs relation is generally valid in the regime accessed by the simulations. In experiments, which typically analyze temperatures close to T_g, the Adam-Gibbs relation seems again to be well obeyed for a range of materials.[10,11,26–32] Yet, experiments as well indicate that the Adam-Gibbs relation does not hold anymore above a temperature scale close to $T_{\rm mct}$,[11,28] in stark contrast with the numerical results. Systematic deviations from the Adam-Gibbs relation were also reported below $T_{\rm mct}$ for some systems,[28,30] but imprecise entropy measurements or inappropriate time scale determinations have been invoked to rationalize them.

In the last three decades, the random first order transition (RFOT) theory of the glass transition[3,5] has revisited the Adam-Gibbs relation in greater depth[4–7] to provide an increasingly precise description of the connection between thermodynamics and dynamics in supercooled liquids. This connection can be decomposed in two steps. First, the decrease in the configurational entropy is shown,

by a purely thermodynamic reasoning,[4] to give rise to a growing "point-to-set" static correlation lengthscale

$$\xi_{\rm pts} \propto S_{\rm conf}^{-1/(d-\theta)}, \tag{2}$$

where an interface exponent θ is introduced. In the simplest approximation, one has $\theta = d - 1$ which corresponds to a (hyper)surface in a space of dimension d. The value $\theta = d/2$ was also proposed[3,7] to take into account finite dimensional surface fluctuations due to the disordered nature of the amorphous phase. More generally, the inequality $\theta \leq d - 1$ is expected to hold. Second, the connection to dynamics is made via the assumption that relaxation in the liquid for $T < T_{\rm mct}$ proceeds via thermally activated events correlated over a lengthscale $\xi_{\rm pts}$, resulting in the general relation[3,4]

$$\log(\tau_\alpha/\tau_0) \propto \xi_{\rm pts}^{\psi}/T, \tag{3}$$

where ψ is a dynamical exponent. Various theoretical and numerical estimates of ψ have been proposed.[4,33–36] In the original paper by Kirkpatrick *et al.*,[3] $\psi = \theta = d/2$ was assumed and so only one exponent had been introduced.

Using Eqs. (2) and (3), one finds a generalized version of the Adam-Gibbs relation,

$$\log(\tau_\alpha/\tau_0) \propto \frac{1}{TS_{\rm conf}^{\alpha}}, \tag{4}$$

with a nontrivial exponent

$$\alpha = \frac{\psi}{d-\theta}. \tag{5}$$

This shows that α may or may not be equal to unity, depending on the relative values of the two independent exponents ψ and θ. As a consequence, Eq. (4) may or may not be equivalent to Eq. (1).

To our knowledge, a direct test of Eqs. (3)–(5) in the theoretically motivated temperature regime, employing appropriate observables, has never been performed. Most previous simulations have considered a temperature regime $T \gtrsim T_{\rm mct}$[12,17,21,37] where the physics is expected to be nonactivated and the configurational entropy and point-to-set lengthscales are not well-defined. This is of course valuable work, but theory itself suggests that the tested scaling relations have no reason to hold in this temperature regime. Experiments instead access the correct temperature regime but cannot easily measure the point-to-set correlation lengthscale. As a proxy, Refs. 38 and 39 replaced $\xi_{\rm pts}$ by the lengthscale of dynamic heterogeneities that can be more easily estimated experimentally.[40] Many other experimental studies study Eq. (1) directly near T_g.[11,30]

In this work, we take advantage of the progress allowed by the swap Monte Carlo algorithm[41,42] to measure directly in several numerical models the temperature dependence of the configurational entropy and point-to-set lengthscale down to T_g. For the dynamics, we build on previous work[42] and provide additional experimental support showing that one can safely estimate the temperature dependence of the relaxation time also down to T_g, using a careful fitting procedure. We collect data from earlier works[43–45] that we extend where needed and perform new simulations for one additional model.

As a result, we are in a position to provide for the first time stringent tests of the Adam-Gibbs relation and of RFOT theory for computer models simulated in the same regime as in experiments. Our results suggest that the Adam-Gibbs relation is generally not valid in computer models in the experimental regime $T_g < T < T_{\rm mct}$. To test our findings against experiments, we collect high-quality thermodynamic and dynamic data for several supercooled liquids (most of which are obtained by state-of-the-art thermodynamic measurements[46]) and reach similar conclusions. Overall, we find that Eq. (1) is not obeyed for most systems, while Eq. (4) is obeyed with an exponent α that fluctuates weakly from system to system with typically $\alpha < 1$. Our findings can be taken as a confirmation either that RFOT theory works well with a nontrivial set of critical exponents or that a small $\alpha < 1$ exponent indicates that thermodynamics is not the only driving force for the dynamic slowdown near T_g.

This paper is organized as follows. In Sec. II, we present the numerical methods used to obtain the configurational entropy, the point-to-set lengthscale, and the relaxation time. We also describe our choice of experimental data to reliably test the Adam-Gibbs relation over a broad range of temperatures. In Sec. III, we present the results of our analysis of the exponents θ and α in simulations and then in experiments. We discuss the physical meaning of our results in Sec. IV.

II. DESCRIPTION OF THE DATA

In order to analyze quantitatively the connection between dynamic and thermodynamic properties, we collect and extend data from previous numerical works. We also collect data from selected published experimental works and motivate our selection.

A. Numerical models

The recent development of the swap Monte Carlo algorithm allows us to access very low-temperature equilibrium configurations in computer simulations. In particular, the temperature regime $T_g < T < T_{\rm mct}$ can be comfortably accessed. This temperature regime is the correct one to test thermodynamic theories as it is precisely where they should apply, and it corresponds to the regime explored experimentally.

We gather simulation data for polydisperse systems using a continuous size distribution.[42] The particle diameters σ are distributed between $\sigma_{\rm min}$ and $\sigma_{\rm max}$ from $f(\sigma) = c\sigma^{-3}$, where c is a normalization constant and $\sigma_{\rm min}/\sigma_{\rm max} = 0.45$. We use the average diameter $\overline{\sigma}$ as the unit length.

We study four numerical models: three-dimensional additive hard spheres (HS3D) and[41] two- and three-dimensional nonadditive soft disks (SSV2D)[43] and spheres (SSV3D)[42] under an isochoric path. We also perform new simulations of three-dimensional nonadditive soft spheres (SSP3D), under an isobaric path. To thermalize the last model, we use an hybrid molecular dynamics/swap Monte Carlo scheme.[47]

We use the following pairwise potential for the polydisperse soft sphere/disk models:[42]

$$v_{ij}(r) = v_0\left(\frac{\sigma_{ij}}{r}\right)^{12} + c_0 + c_1\left(\frac{r}{\sigma_{ij}}\right)^2 + c_2\left(\frac{r}{\sigma_{ij}}\right)^4, \tag{6}$$

$$\sigma_{ij} = \frac{(\sigma_i + \sigma_j)}{2}(1 - \epsilon|\sigma_i - \sigma_j|), \tag{7}$$

where v_0 is the energy unit and ϵ quantifies the degree of nonadditivity of the system. We set $\epsilon = 0.2$ for SSV3D and SSV2D, and $\epsilon = 0.1$ for SSP3D. The constants, c_0, c_1, and c_2, are chosen to smooth $v_{ij}(r)$ up to its second derivative at the cut-off distance $r_{cut} = 1.25\sigma_{ij}$. We set the number density $\rho = N/L^3 = 1.02$ with $N = 1500$ for SSV3D and $\rho = N/L^2 = 1.01$ with $N = 1000$ for SSV2D. For SSP3D, the pressure on the isobaric path is $P = 30.0$. For HS3D,[41] the pair interaction is zero for nonoverlapping particles and infinite otherwise. The relevant control parameter for hard spheres is the reduced pressure $p = P/(\rho T)$. For hard spheres, $1/p$ plays precisely the same role as temperature T for a dense liquid,[48] and there is no distinction between isochoric and isobaric paths.

Relaxation times for HS3D, SSV3D, and SSV2D are measured in units of MC sweeps, which comprise N Monte Carlo trial moves. For SSP3D, the relaxation time is expressed in units of $\sqrt{v_0/m\bar{\sigma}^2}$, where m is the mass of the particles.

B. Configurational entropy and point-to-set length

The configurational entropy S_{conf} is measured from configurations generated with swap Monte Carlo simulations. It is defined as $S_{conf} = S_{tot} - S_{glass}$, where S_{tot} and S_{glass} are the total and glass entropies, respectively.[16] S_{tot} and S_{glass} are computed using thermodynamic integration schemes, as explained in Ref. 45. In Appendix A, we describe how to measure S_{conf} along an isobaric path using constant pressure simulations for SSP3D as this was not documented before.

Figure 1 shows the configurational entropy that we use for latter analysis. The data for $S_{conf}(T)$ are normalized by the values at the mode coupling crossover T_{mct}, whose value is determined by a power law fit to the dynamic relaxation time data.[25] The actual values are $T_{mct} = 0.0426$, 0.104, 0.556, and 0.123 for HS3D, SSV3D, SSP3D, and SSV2D, respectively.

In order to increase the accuracy of the analysis, we employ empirical fitting functions. For the three-dimensional models, we use a conventional fitting function plus a quadratic correction, $TS_{conf} = A(T-T_K)+B(T-T_K)^2$.[11,49] For the two-dimensional model, we use $1/S_{conf} = A/T + B$.[43] These fitting functions conveniently enable us to incorporate S_{conf} values in between actual data points and help us determining the exponents. The fitting parameters are presented in Table I.

We also collect the point-to-set lengthscale ξ_{pts} data for SSV2D[43] and HS3D,[44] obtained from recently developed computational methods.[50,51] Together with S_{conf}, the data for ξ_{pts} will allow us to estimate the exponent θ using Eq. (2).

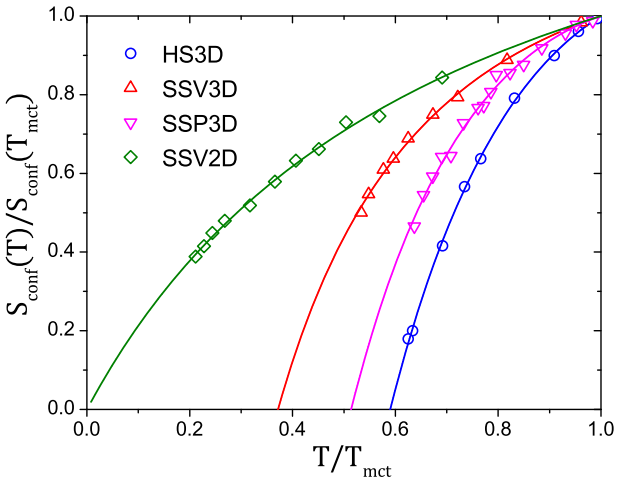

FIG. 1. Configurational entropy data for the four simulated models. The data are normalized by the values at the mode coupling crossover T_{mct}. The solid curves represent the fitting functions defined in the text and Table I.

C. Relaxation times

Dynamical information is obtained using either standard Monte Carlo (for HS3D, SSV3D, SSV2D) or molecular dynamics (for SSP3D). The equivalence between the two types of dynamics is well documented.[52] Both Monte Carlo and molecular dynamics simulations are run starting from initial configurations that are obtained using the swap Monte Carlo algorithm. This procedure allows us to cover about 5 orders of magnitude of relevant slow dynamics.

The relaxation time τ_α is measured by the self-intermediate scattering function in three dimensional models. For the two-dimensional model, we use the autocorrelation function of the bond-orientational order parameter, which is insensitive to the long-range Mermin-Wagner fluctuations that are specific to $d = 2$.[53]

The relaxation time τ_α for HS3D,[44] SSV3D,[42] SSP3D (new to this work), and SSV2D[43] is shown in Fig. 2. The data are normalized using an onset temperature T_o for the emergence of slow dynamics, determined from the fitting procedure described below, and define $\tau_o = \tau_\alpha(T = T_o)$. Clearly, all simulation data show a non-Arrhenius temperature dependence of the relaxation time, which demonstrates that our models describe fragile glass-formers.

The swap numerical schemes allow us to prepare equilibrated configurations at very low temperatures. Because they involve non-physical particle dynamics, one cannot use them to measure the relaxation time of the physical dynamics in this low-temperature regime. Therefore, we need to extrapolate the relaxation time from the regime where τ_α can be measured to the experimental regime, where this is unachievable.

We start by employing the Vogel-Fulcher-Tammann (VFT) law

$$\log(\tau_\alpha/\tau_0) \propto (T - T_{VFT})^{-1}, \tag{8}$$

where τ_0 and T_{VFT} are fitting parameters. We fitted this function on our numerical data over the accessible time window, and we

TABLE I. Fitting parameters for the configurational entropy (A, B, and T_K), for the relaxation time (τ_o, T_o, and C), and kinetic fragility index m for the simulated models. Note that Monte Carlo dynamics (HS3D, SSV3D, SSV2D) and molecular dynamics (SSP3D) have different time units.

Model	A	B	T_K	$\log_{10}\tau_o$	T_o	C	m
HS3D	3.209	−37.33	0.0251	3.89	0.063	22.72	45.5
SSV3D	1.495	−1.92	0.0387	3.02	0.266	3.15	32.0
SSP3D	2.082	−1.74	0.2902	0.41	0.961	16.77	42.4
SSV2D	0.073	0.84	...	2.40	1.006	0.25	31.2

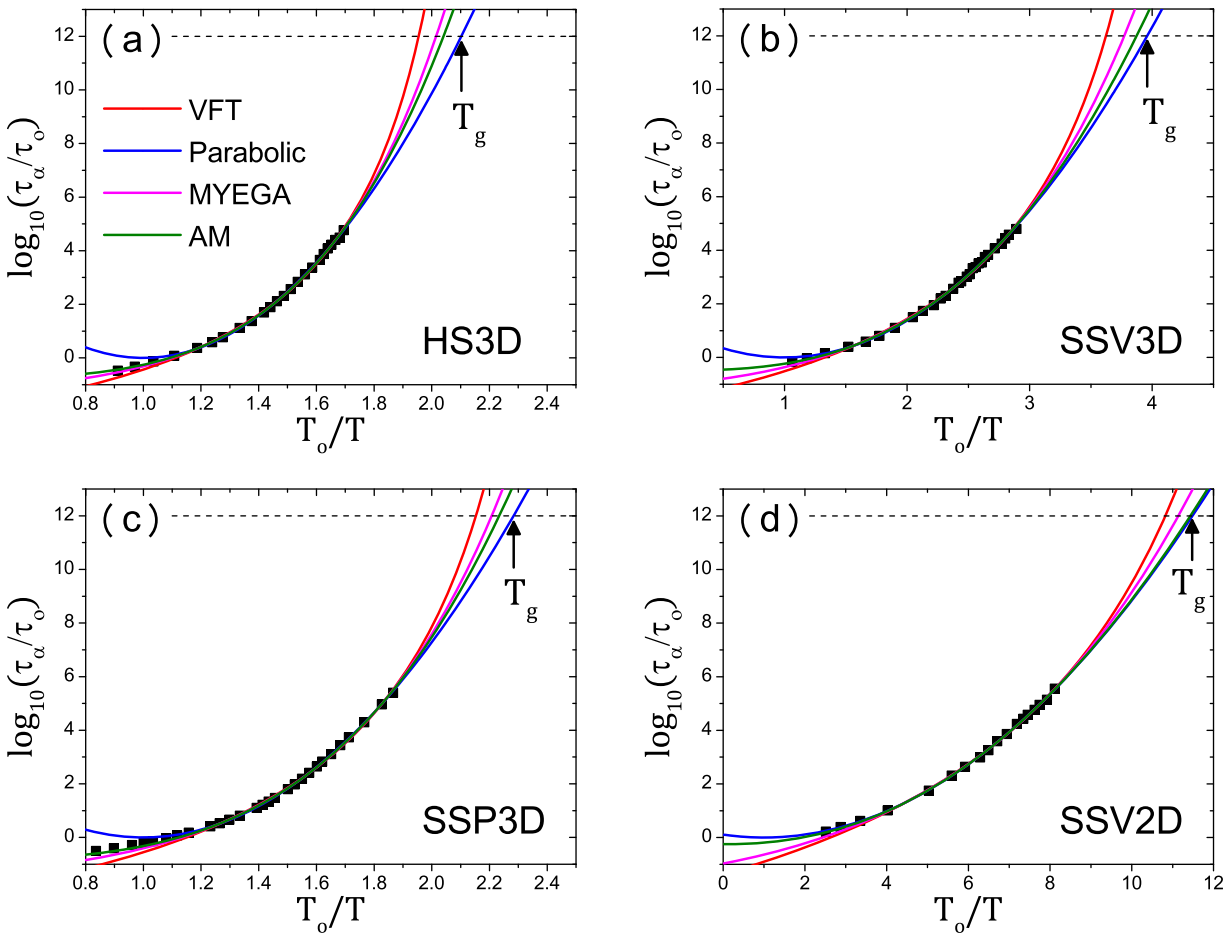

FIG. 2. Relaxation time as a function of inverse temperature for the four simulated models: HS3D (a), SSV3D (b), SSP3D (c), and SSV2D (d). The data are normalized by τ_o and T_o, determined from a parabolic-law fitting. The horizontal dashed line indicates the time scale of the experimental glass transition, $\tau_\alpha/\tau_o = 10^{12}$. The vertical arrow indicates the experimental glass transition temperature T_g using the parabolic-raw fitting. Three additional fitting functions are shown.

concluded that it performs very badly when extrapolated at lower temperatures. We found, for instance, that the swap Monte Carlo algorithm easily thermalizes at temperatures below the extrapolated VFT critical temperature T_{VFT}, which invalidates directly its use to describe numerical data.[42] The inability of the VFT law to describe experimental data over a wide range of temperature was discussed in detail in Refs. 54 and 55.

It has been found in previous experimental studies that the parabolic law

$$\tau_\alpha^{\mathrm{para}} = \tau_o \exp[C(T_o/T - 1)^2] \tag{9}$$

fits accurately the data over a very large temperature range.[56] Its fitting parameters are τ_o, C, and T_o.

In addition to the VFT and parabolic laws, we consider two other functional forms, shown in Fig. 2. One is a double exponential equation (MEYGEA) discussed in Refs. 56 and 57,

$$\tau_\alpha = \tau_0 \exp\left[\frac{K}{T}\exp[C/T]\right], \tag{10}$$

where τ_0, K, and C are the fitting parameters. The other one is the Avramov and Milchev (AM) equation[58] given by

$$\tau_\alpha = \tau_0 \exp[A/T^n], \tag{11}$$

where τ_0, A, and n (real exponent) are the fitting parameters. All the fitting functions considered in this paper have three free-fitting parameters which is the minimal number to mathematically characterize non-Arrhenius behavior. Given the small variation of the apparent activation energy over the dynamic range studied experimentally, it is not surprising that several smooth functions of temperature can describe the evolution of $\log(\tau_\alpha)$. Figure 2 shows that different fitting functions produce slight variations in the extrapolated value for T_g. The key issue is therefore to choose the best fitting function, i.e., the one from which the low temperature data can be inferred accurately from the high temperature one.

To find the best fitting procedure, we train on experimental data (see Appendix B). We fit the above four equations to the data, restricting ourselves to a modest dynamic range, comparable to

numerical time scales. We then extrapolate to temperatures close to T_g and compare the extrapolation to the actual data. We find excellent agreement when using the parabolic law for the experimental data with kinetic fragility indexes similar to our numerical models, which validates further our procedure. Thus, we empirically find that fitting the parabolic law to the numerical time window provides an excellent description of the data close to T_g, as reported previously.[56] This is a purely practical choice, and we make no assumption about the physical mechanism which could lead to such a law.

By using the fitting parameter τ_o obtained from the parabolic law, we define two time windows. First, we define the *simulation window* by $\tau_\alpha/\tau_o \in [10^0, 10^5]$. The upper bound of this time scale corresponds to recent simulation studies with very long time scales.[44,59] The *experimental window* is defined by $\tau_\alpha/\tau_o \in [10^3, 10^{12}]$. The lower bound corresponds to a time scale around the mode-coupling crossover $T_{\rm mct}$ ($\tau_\alpha \simeq 10^{-7}$ s[60]), and the upper bound corresponds to the time scale at the experimental glass transition T_g ($\tau_\alpha \simeq 100$ s). The experimental window is therefore the appropriate regime to test the predictions made by the RFOT theory. Notice that in this paper, we try neither to go below T_g nor to examine the fate of supercooled liquids at even lower temperature.[61]

For numerical models, we determine the experimental glass transition temperature $T_{\rm g}$ as $\tau_\alpha^{\rm para}(T_{\rm g})/\tau_o = 10^{12}$. The kinetic fragility index m is determined by $m = \partial \log_{10} \tau_\alpha^{\rm para}/\partial(T_{\rm g}/T)|_{T=T_{\rm g}}$. The fitting parameters and fragility indexes are given in Table I.

D. Experimental data

We select materials for which high-quality data for the configurational entropy and relaxation time over a broad temperature range is available in the literature. This allows for a comparison with computer simulations and an accurate determination of the exponent α in Eq. (4).

We select 2-methyl tetrahydrofuran (2MTHF), ethylbenzene (ETB), ethanol, glycerol, *o*-terphenyl (OTP), 1-propanol, propylene carbonate (PC), salol, toluene, and 3-bromopentane. The configurational entropy data for 2MTHF, ETB, OTP, PC, salol, and toluene were recently obtained from accurate experiments by Tatsumi, Aso, and Yamamuro. Some of the data are presented in Ref. 46. The data for 1-propanol are taken from Ref. 62. In these data for all the above materials, $S_{\rm conf}$ is measured by thermodynamic integration of the heat capacity difference between supercooled liquids and nonequilibrium glasses. This treatment should be conceptually better than using the crystal entropy,[11] but this is still a rather crude approximation,[63] whose accuracy is expected to be material-dependent.[64] For ethanol,[65,66] glycerol,[65,67] and 3-bromopentane,[27] $S_{\rm conf}$ is obtained using the crystal entropy $S_{\rm cry}$, i.e., $S_{\rm conf} = S_{\rm liq} - S_{\rm cry}$. Notice that we do not seek to present thermodynamic data for ultrastable glasses prepared below T_g even though we believe that these materials can be instrumental to test more precisely glass transition theories.[68]

The relaxation time data are mainly obtained from dielectric measurements, but some data are combined with other methods, such as viscosity measurements. The corresponding references are 2MTHF,[11] ETB,[69–71] ethanol,[46] glycerol,[72–74] OTP,[75] 1-propanol,[11,76,77] PC,[73,74,78] salol,[79] toluene,[75] and 3-bromopentane.[80]

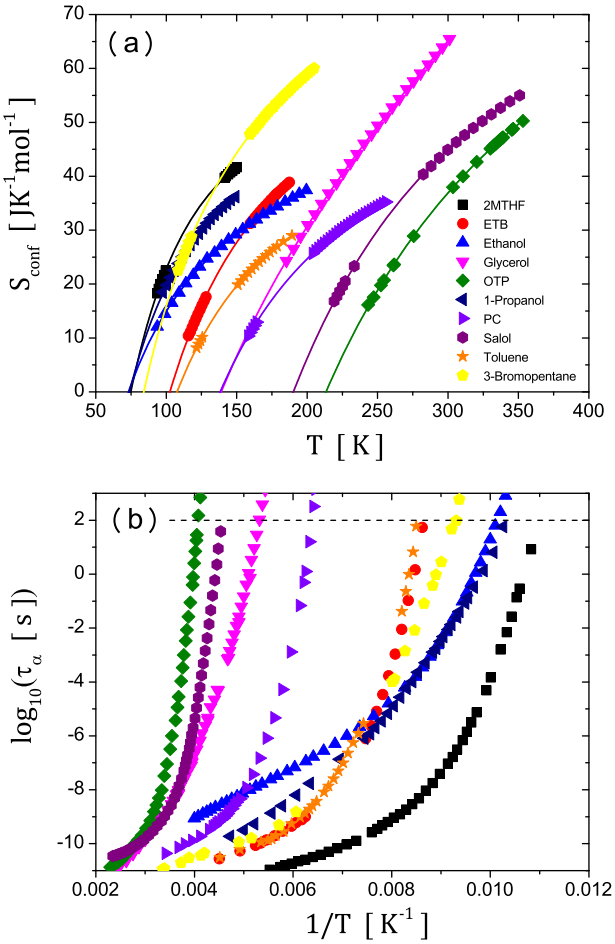

FIG. 3. (a) Configurational entropy data for 2MTHF,[46] ETB,[46] ethanol,[66] glycerol,[67] OTP,[81] 1-propanol,[62] PC,[46] salol,[81] toluene,[46] and 3-bromopentane.[27] The solid curves are quadratic fitting functions as used for the $d = 3$ numerical models. (b) Relaxation time data for 2MTHF,[11] ETB,[69–71] ethanol,[82] glycerol,[72–74] OTP,[75] 1-propanol,[11,76,77] PC,[73,74,78] salol,[79] toluene,[75] and 3-bromopentane.[80] The horizontal dashed line indicates the time scale of the experimental glass transition, $\tau_\alpha = 100$ s.

For the experimental data, we set $\tau_o = 10^{-10}$ s. Therefore, the simulation and experimental time windows correspond to $\tau_\alpha \in [10^{-10}$ s, 10^{-5} s] and $\tau_\alpha \in [10^{-7}$ s, 10^2 s], respectively. In particular, T_g corresponds to the standard relaxation time $\tau_\alpha = 100$ s.

The configurational entropy and relaxation time data for the materials presented above are gathered in Fig. 3 together with empirical quadratic fits to the configurational entropy.

III. RESULTS

In this section, we perform a test of Eqs. (1)–(5) using the experimental and numerical data presented in Sec. II. We first study Eq. (2) using numerical data for $\xi_{\rm pts}$ and $S_{\rm conf}$ to estimate θ. Then, we estimate α in Eq. (4) by comparing τ_α and $S_{\rm conf}$ using both computer simulations and experiments to investigate the validity of the

Adam-Gibbs relation in Eq. (1). Finally, the values of θ and α allow us to discuss that taken by $\psi = (d - \theta)\alpha$, deduced from Eq. (5).

A. The static exponent θ

First, we estimate the exponent θ in Eq. (2) combining independent data obtained for S_{conf} and ξ_{pts}.

Figure 4 shows a log-log plot of S_{conf} vs ξ_{pts} for three dimensional polydisperse hard spheres (HS3D) (a) and two dimensional soft disks (SSV2D) (b). We use the fitted functional form for S_{conf} (obtained in Fig. 1), whereas the actual data points are used for ξ_{pts}. We emphasize that while temperature is a running parameter in this plot, the data point in Fig. 4 correspond to the regime of interest $T < T_{mct}$. Such results have never been achieved as earlier numerical work were all performed for $T > T_{mct}$ or only slightly below T_{mct}.[33] Despite the larger temperature range explored in this work, we are fully aware that the relative variation of ξ_{pts} and S_{conf} remains fairly modest, which makes the determination of a critical exponent quite difficult.

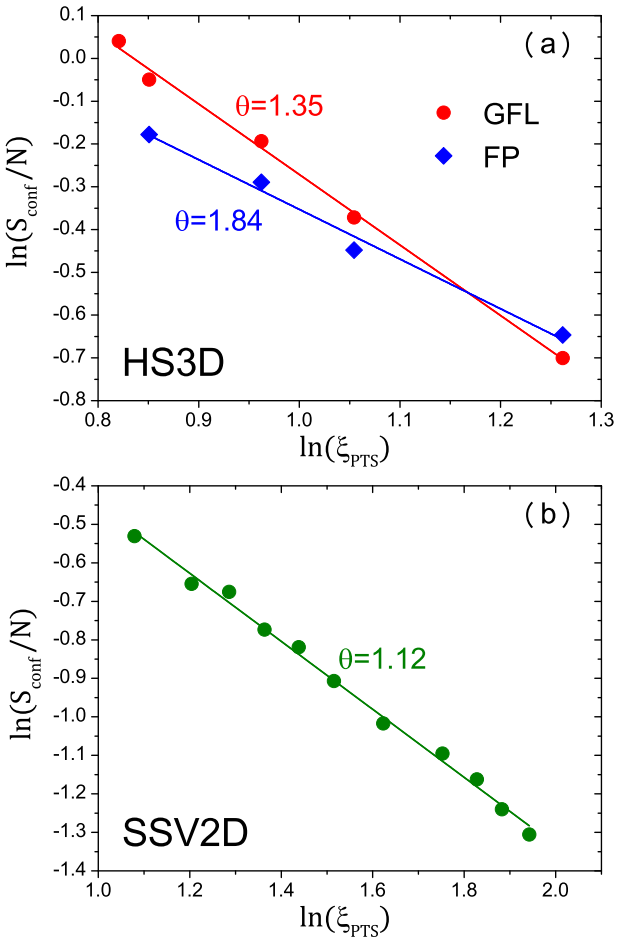

FIG. 4. S_{conf} vs ξ_{pts} plot in $d = 3$ hard spheres (HS3D) (a) and $d = 2$ soft disks (SSV2D) (b). The straight lines are power law fits. For HS3D, we show two independent estimates of S_{conf} obtained from the generalized Frenkel-Ladd (GFL) method and the Franz-Parisi (FP) free energy approach.

For HS3D, we report two estimates for S_{conf}, obtained from different schemes. One is a generalized Frenkel-Ladd (GFL) method,[45,83] and the other is the Franz-Parisi (FP) free energy method proposed earlier.[44,84,85] The exponent θ is extracted by fits to straight lines, whose slope gives $\theta - d$; see Eq. (2). We obtain $\theta = 1.35 \pm 0.06$ for GFL and $\theta = 1.84 \pm 0.09$ for FP. These values are compatible with either the theoretical prediction $\theta = d/2$ by Kirkpatrick *et al.*[3] or with that of Franz $\theta = d - 1$.[86]

We obtain $\theta = 1.12 \pm 0.02$ for SSV2D. This value is close to both theoretical predictions, $\theta = d/2$ and $\theta = d - 1$, which coincide in $d = 2$, giving $\theta = 1$. Obviously, one cannot discriminate between the two predictions.

Overall, we find that for $d = 3$, the value measured for θ conforms with the two available predictions, which is an encouraging result from the viewpoint of RFOT theory. Unfortunately, the obtained values fall in-between the two predictions, which are too close to be discriminated. We suggest that performing point-to-set and configurational entropy measurements in $d = 4$, combining recently developed tools,[45,51,87] would be very useful to conclude on this point. Indeed, when $d = 4$, the two predictions yield $\theta = d/2 = 2$ and $\theta = d - 1 = 3$, which are further apart than in $d = 3$.

B. Breakdown of the Adam-Gibbs relation and numerical estimation of α

We next examine the validity of Eq. (4) by connecting τ_α and S_{conf} and estimating the exponent α. When $\alpha = 1$, the Adam-Gibbs relation in Eq. (1) is recovered.

In Figs. 5(a), 5(c), 5(e), and 5(g), we show conventional Adam-Gibbs plots where the evolution of $\log_{10}(\tau_\alpha/\tau_o)$ is represented as a function of $1/(Ts_{conf})$, where $s_{conf} = S_{conf}/N$, for hard spheres (HS3D) (a), soft spheres along the isochoric path (SSV3D) (c), along the isobaric path (SSP3D) (e), and the soft disks (SSV2D) (g). We combine the dynamic and thermodynamic data described in Sec. II, restricted to the experimental time window ($\tau_\alpha/\tau_o \in [10^3, 10^{12}]$). We use the fitted functional forms for both τ_α (estimated in Fig. 2) and S_{conf} (obtained in Fig. 1), which produces "continuous curves" instead of a discrete data points. To our knowledge, this is the first time that the Adam-Gibbs relation is tested for computer models over the time window where it is actually supposed to apply.

For all three-dimensional models, we find that $\log_{10}(\tau_\alpha/\tau_o)$ is a concave function of $1/Ts_{conf}$, whereas it is convex for the two-dimensional model. If tested over a narrow time window close to T_{mct}, an acceptable linear behavior could possibly be observed, which would suggest the validity of the Adam-Gibbs relation, in agreement with many earlier findings.[12,17–24] The trend that we report here appears to contrast with recent results obtained in the Kob-Andersen model, where slight convexity and concavity are, respectively, observed in $d = 3$[23] and $d = 2$.[21] These results were however obtained in the numerical time window, above T_{mct}. Our results demonstrate that when observed over a much broader range and closer to T_g, the Adam-Gibbs relation is actually not obeyed for any of the numerical models studied here.

The clear violations of the standard Adam-Gibbs relation that we find over the experimental time window imply that the exponent α must deviate from the value $\alpha = 1$. We varied its value around unity and used it as a free parameter to obtain generalized Adam-Gibbs plots, which are shown in Figs. 5(b), 5(d), 5(f), and 5(h) for

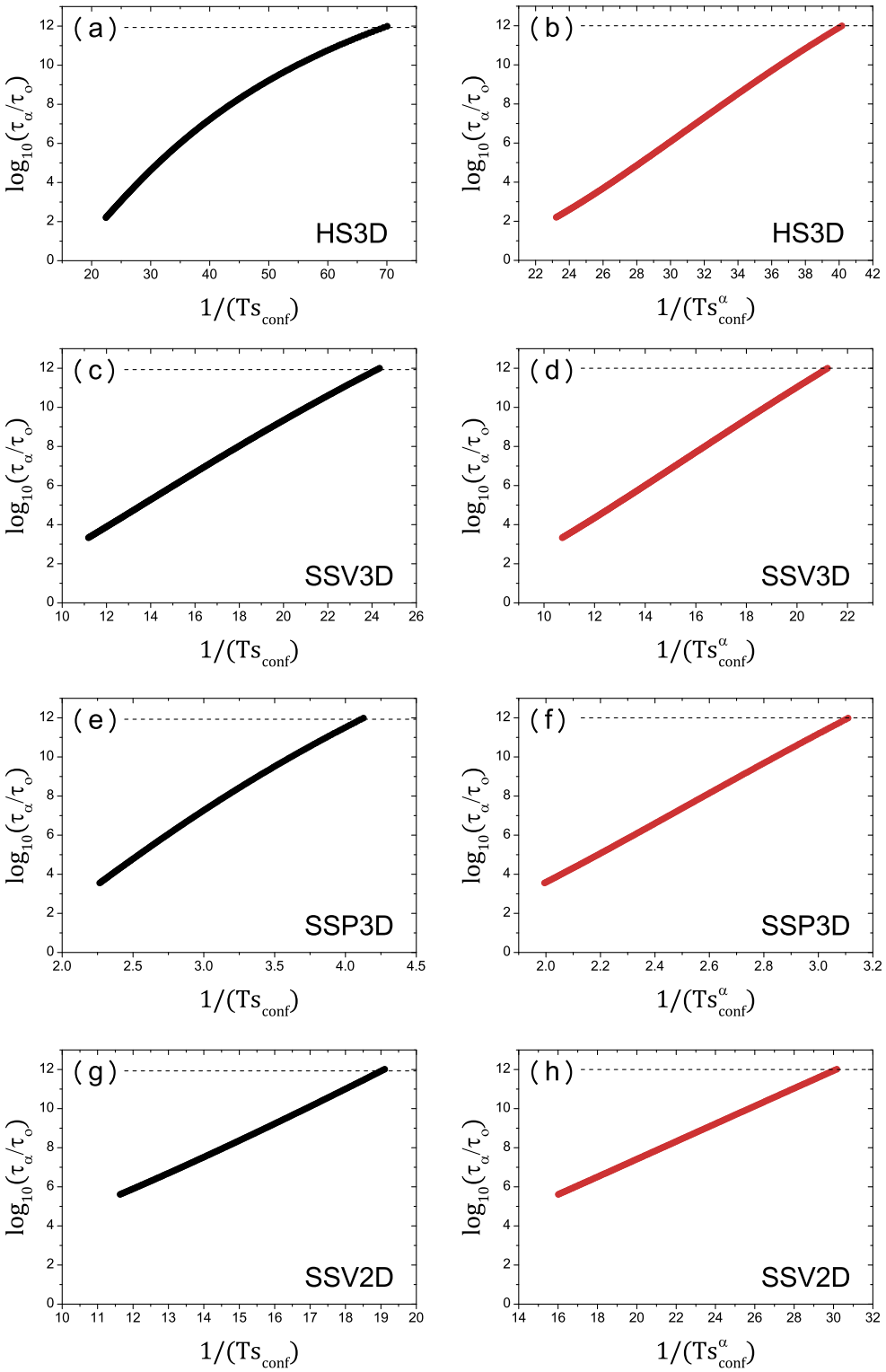

FIG. 5. Left panels: Standard Adam-Gibbs plot for the d = 3 hard spheres (HS3D) (a), d = 3 soft spheres along the isochoric path (SSV3D) (b), the isobaric path (SSP3D) (c), and d = 2 soft disks (SSV2D) (d). Right panels: Generalized Adam Gibbs plots with the fitted α value for each model for HS3D (b), SSV3D (d), SSP3D (f), and SSV2D (h). The horizontal dashed lines correspond to the time scale for the experimental glass transition T_g.

the same numerical models. All plots now show a perfect straight line, suggesting that the introduction of the parameter α is sufficient to describe the data. We obtain α = 0.24, 0.49, 0.72, and 1.89 for HS3D, SSP3D, SSV3D, and SSV2D, respectively, so that $\alpha < 1$ for the three dimensional models, whereas $\alpha > 1$ for the two dimensional model.

Since the four models we have simulated all display violations of the Adam-Gibbs relation, we conclude that Eq. (1) does not describe well the physics of simulated supercooled liquids when analyzed over the experimental time window. Additional models should be studied and analyzed before concluding about the possible universality of the exponent α, but our initial results do not point toward a constant value. Once more, it would be very valuable to obtain data in $d = 4$ to see if a different value for α is found in larger spatial dimensions.

C. Breakdown of the Adam-Gibbs relation and experimental estimation of α

Before starting this study, we felt that there was a general consensus in the community that the Adam-Gibbs relation is well-obeyed in real materials analyzed near the experimental glass transition T_g. Thus, the outcome of the computer simulations showing deviations from Eq. (1) appeared as a worrying disagreement between simulations and experiments.

Therefore, we decided to collect data sets for several molecular liquids, where high-precision dynamic and thermodynamic data would be available over both simulation and experimental time windows in order to perform a direct comparison with computer models.

We present the results of our data collection in Fig. 6(a) using again the representation where the standard Adam-Gibbs relation would yield a straight line. We use the fitted functional form for $S_{\rm conf}$ [obtained in Fig. 3(a)], whereas the actual data points are used for τ_α. When analyzed over the entire experimental time window, defined above, we again observe a clear concavity for most materials. The Adam-Gibbs relation in Eq. (1) is violated over this regime although, of course, it holds if observed over a restricted time window close to T_g[11] (almost by definition—the data are continuous!).

As for the simulations, we fit the experimental data using the exponent α as an additional free parameter. From the experimental data, we determine two distinct values for α, obtained by fitting either over the simulation or the experimental time window. The typical trend that we observe is that $\alpha > 1$ over the simulation time window, but $\alpha < 1$ over the experimental time window. The latter fits are included in Fig. 6(a), and they describe well the data over the entire experimental time window. As with the case for the simulation models, in Fig. 6(b), we also present the generalized Adam-Gibbs plot with the fitted α value for each material in the experimental time window. We confirm that the linear behavior is recovered in this plot.

We notice that the concavity in the Adam-Gibbs plot in the experimental time window was already reported.[28,30] However, the concavity would be overlooked as it is less pronounced than the convexity found at much higher temperature, close to $T_{\rm mct}$ and above.[28] Moreover, Ref. 30 concluded that the observed concavity was attributed to an imprecise estimate of the configurational entropy. Our results obtained from simulation data with accurate configurational entropy measurements and recent high-quality experimental data suggest instead that the observed concavity is a generic physical phenomenon reflecting the nature of glassy dynamics over the experimental time window.

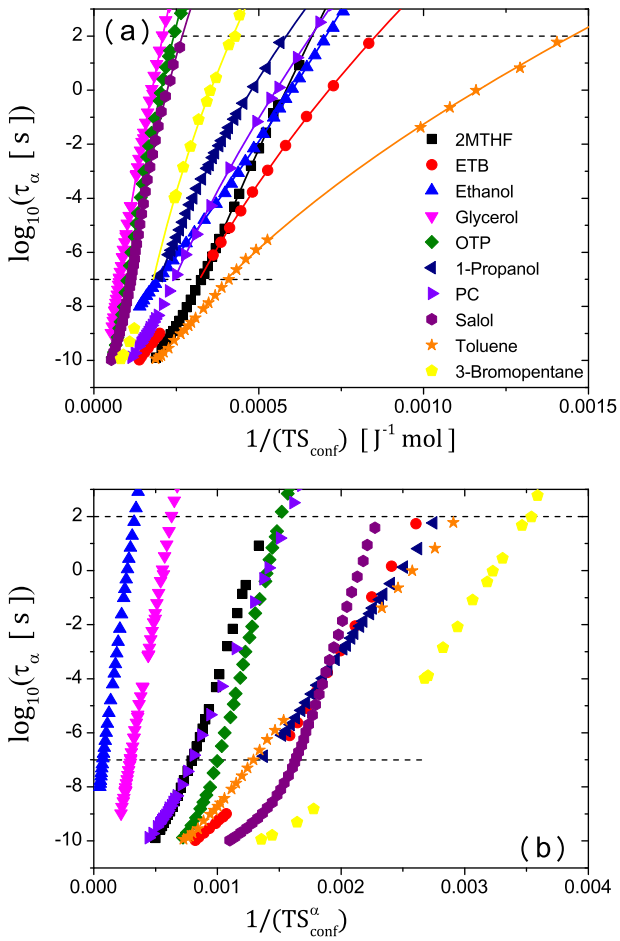

FIG. 6. (a) Standard Adam-Gibbs plot constructed from experimental data all except ethanol display a concave behavior. The solid curves correspond to fits using Eq. (4) using α as a fit parameter over the experimental time window. (b) Generalized Adam Gibbs plots with the fitted α value for each material. The horizontal dashed lines indicate the time scale of the experimental glass transition, τ_α = 100 s, and the lower bound of the experimental time window, $\tau_\alpha = 10^{-7}$ s.

IV. DISCUSSION

Our central conclusion from both simulations and experiments considered over a broad time regime $\tau_\alpha/\tau_o \in [10^3, 10^{12}]$ (defined to be both experimentally accessible and theoretically relevant) is that the conventional Adam-Gibbs relation in Eq. (1) is not obeyed. Instead, the general form predicted by RFOT theory in Eq. (4) describes numerical and experimental data well. This is maybe not so surprising, from an empirical viewpoint, given that the generalized relation has one more free fitting parameter.

We compile all our results for the values of α from simulations (empty points) and experiments (filled points) in Fig. 7. To organize the data, we use the kinetic fragility index m as the horizontal axis. This is simply a matter of convenience (as a matter of fact, no strong trend is observed). Note that, somewhat paradoxically, we do not have values for α in the computer models over the simulation time window because our computational schemes to measure S_{conf} only become applicable for low enough temperatures, typically $T \lesssim T_{mct}$.[45,85]

The experimental data in Fig. 7 obtained by considering the simulation time window are dispersed, $\alpha = 0.73–2.34$, and tend to be characterized by rather large values $\alpha > 1$. By contrast, considering a broader and physically better justified experimental time window, data for both simulations and experiments are much less scattered, $\alpha \simeq 0.24–1.28$, with a preferred average value $\alpha \simeq 0.5–0.6$, except for ethanol.

Before concluding, we make a further caveat regarding the above analysis of the RFOT theory predictions. In principle, we could have introduced additional subdominant physical prefactors into the scaling relations in Eqs. (2) and (3) that could also be temperature dependent quantities. In particular, a surface tension could enter the relation between S_{conf} and ξ_{pts},[6,88] and an energy scale could enter the activated scaling relation in Eq. (3). These prefactors would become irrelevant if some asymptotic regime could be reached with extremely long relaxation times and very small configurational entropy values, but it is understood that experimental glasses are not in this regime.[89] In the absence of strong theoretical insights into these quantities, we decided to ignore them. They could of course very well affect the measured values of the reported exponents. Thus, a better determination of these quantities is an important research goal,[33,90,91] in particular, in the experimental time window.

We also discuss potential sources of uncertainty in terms of experimental measurements of τ_α and S_{conf}, whose accuracy would affect the determination of the scaling exponent α. Regarding τ_α, we note that the dielectric relaxation measurement for ethanol involves a Debye relaxation process which is distinct from the structural α relaxation process as recently clarified in an experiment.[92] Indeed, the relaxation time extracted from the main peak that we used in this paper[82] corresponds to the former process in ethanol, whereas we should instead use the α relaxation process, but it is also found that the overall temperature dependence of two relaxation processes are very similar.[92] It could be that the unusual behavior in ethanol, showing $\alpha > 1$, is related to this issue.

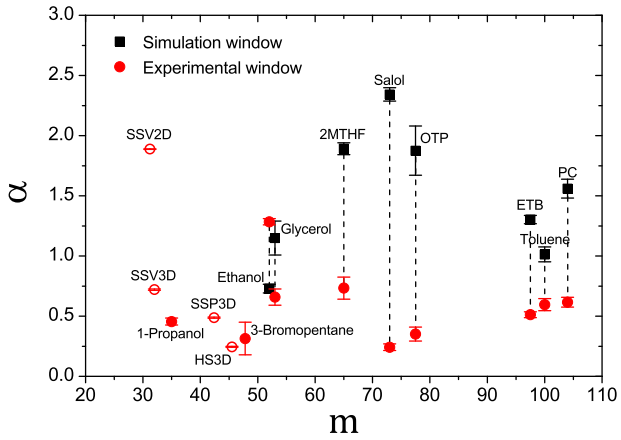

FIG. 7. The measured values of α presented, for convenience, as a function of the kinetic fragility index m for the simulation (black squares) and experimental (red circles) time windows for various materials. The errorbars correspond to the standard error for the fit. The vertical dashed lines connect the two values for each material. Empty circles correspond to simulation models where α is measured over the experimental time window only.

The experimental measurement of S_{conf} also involves approximations. First, using the excess entropy, $S_{exe} = S_{liq} - S_{cry}$, instead of $S_{conf} = S_{liq} - S_{glass}$ is an approximation, in general. The validity of $S_{glass} \approx S_{cry}$ has been widely studied,[64,93–99] and it seems to be nonuniversal.[64] Typically, S_{glass} is determined from the heat capacity of the nonequilibrium glass state, and so it still involves some approximations compared to its theoretical definition.[63] Second, the measurements of S_{conf} in Ref. 46 were performed by doping the different materials to avoid crystallization. In particular, measurements for toluene and ETB involve 10 wt. % doping with benzene. Therefore, mixing effects possibly contribute to the absolute value of S_{conf} and to its temperature dependence.[100]

To summarize our results in terms of numerical values for the critical exponents introduced within RFOT theory, we observe in $d = 3$ that the combination $\theta \simeq 3/2$ and $\alpha \simeq 0.5–0.6$ works well, which would then result in ψ falling in the range $\psi \simeq 0.75–0.90$. If we use instead the value $\theta = 2$, we would obtain a somewhat larger value for the dynamic exponent $\psi \simeq 1.0–1.2$, which agrees well with earlier indirect analysis.[38,39] Both values violate the general bound $\psi \geq \theta$ discussed in the context of spin glasses,[101] the equality $\psi = \theta$ found for the random field Ising model,[102] and the prediction $\psi = \theta = d/2$ in Ref. 3. In the absence of stronger theoretical constraints, we tentatively conclude that the measured ψ value that we observe appears somewhat small, i.e., smaller than all known theoretical predictions. In $d = 2$, we get $\theta \simeq 1.1$ and $\alpha \simeq 1.9$, which in turns implies that $\psi \simeq 1.7$, which appears somewhat large, by contrast with $d = 3$.

Our conclusion that $\alpha < 1$ is favored by the data over the experimental time window sheds some new light on an old debate in the glass literature.[5,56,103,104] Assuming the existence of an ideal glass transition at equilibrium where $S_{conf} \to 0$ and $\tau_\alpha \to \infty$, one is naturally led to the determination of two critical temperatures: the Kauzmann temperature T_K where S_{conf} vanishes, and the critical temperature T_0 where the relaxation time diverges (not to be confused with onset temperature T_o used above). Typically, the latter is obtained from a Vogel-Fulcher-Tammann fit [$T_0 = T_{VFT}$ in Eq. (8)] to the relaxation time. The possible equality $T_0 = T_K$ would provide a strong empirical sign for the existence of an ideal glass transition underlying glass formation.[5] A large data set collected by Tanaka suggests the existence of systematic differences between the two temperatures,[103] with the tendency that $T_K > T_0$, and an apparent correlation with kinetic fragility. In our analysis using Eq. (4) to describe the data, the connection between thermodynamics and dynamics becomes automatically satisfied, and thus by construction thermodynamic and dynamic, singularities necessarily coincide. Assuming that the determination of T_K is the most robust one, we conclude that it is the experimental determination of T_0 which should be questioned. In particular, using $\alpha < 1$ in Eq. (4)

and assuming an asymptotically linear vanishing of S_{conf}, one would predict that $\log(\tau_\alpha/\tau_0) \propto (T - T_0)^{-\alpha}$, which is distinct from the standard Vogel-Fulcher-Tamman fit and would automatically produce the equality $T_K = T_0$.

From a broader perspective, we conclude that the Adam-Gibbs relation, which is an important milestone in the field of glass transition studies, is generally violated in both computer models and real materials when tested over a broad, experimentally relevant temperature range. We nevertheless argued that the failure of Eq. (1) cannot be taken as evidence that thermodynamic theories of the glass transition are incorrect. The RFOT theory prediction of a connection between statics and dynamics in Eq. (4) is obeyed by all materials, with exponent values that are reasonable, but remain to be predicted from first principles. A larger concern, perhaps, is the apparent lack of universality in the data shown in Fig. 7 which clearly display variations from one system to another. This may still be rationalized by invoking the fact that α is obtained from the analysis of a finite time window where additional preasymptotic effects and temperature dependent prefactors may influence the reported results.

Taking an orthogonal perspective, we finally ask the following: Do our results validate or invalidate some theories of the glass transition? After all, we just established that a slightly generalized version of the Adam-Gibbs relation with $\alpha \simeq 0.6$ describes simulations and experiments over 9 orders of magnitude in the experimentally relevant regime. This is not a small accomplishment. One can take the alternative view that the deviations from the canonical exponent values should be taken as an indirect sign that thermodynamics only contributes some part of the slowing down, in addition to other physical factors.[105–110] This view is sometimes also invoked to rationalize the "modest" growth of static correlation lengthscale observed numerically and experimentally.[89,111] Our finding that $\alpha < 1$ suggests instead that it is the growth of the relaxation time that is actually too modest! It is therefore difficult to rationalize how another physical factor working in addition to the entropy could be invoked to explain our findings. The most radical view is in fact that thermodynamics is just a spectator to the glassy dynamics,[112] in which case our findings should be interpreted as purely coincidental since entropy plays in fact no role. We have no strong argument to oppose this view, which remains perfectly admissible.

ACKNOWLEDGMENTS

We thank J.-P. Bouchaud, D. Coslovich, and F. Zamponi for insightful discussions. We also thank S. Tatsumi and O. Yamamuro for sharing their high-quality experimental data for the configurational entropy. The research leading to these results has received funding from the Simons Foundation (Grant No. 454933, Ludovic Berthier).

APPENDIX A: CONFIGURATIONAL ENTROPY ALONG AN ISOBARIC PATH

We wish to measure the configurational entropy $S_{conf}(T, P)$ along an isobaric (constant pressure) path. It is computed as $S_{conf}(T, P) = S_{tot}(T, P) - S_{glass}(T, P)$, where $S_{tot}(T, P)$ and $S_{glass}(T, P)$ are the total and glass entropies at the temperature T and pressure P. We explain how to get $S_{conf}(T, P)$ from NPT simulation trajectories.

1. Notations

We consider the Helmholtz free energy $-\beta F(T, V) = \ln Z(T, V)$, where $\beta = 1/T$ and $Z(T, V)$ is the partition function of the NVT ensemble. We also consider the Gibbs free energy $-\beta G(T, P) = \ln Y(T, P)$, where $Y(T, P)$ is the partition function of the NPT ensemble, given by

$$Y(T,P) = \int_0^\infty \mathrm{d}V e^{-\beta(PV+F(T,V))}. \tag{A1}$$

We introduce the probability distribution of the volume V for a given T and P,

$$\rho(V|T,P) = \frac{e^{-\beta(PV+F(T,V))}}{Y(T,P)}. \tag{A2}$$

In equilibrium, $\rho(V|T, P)$ is given by the Gaussian distribution

$$\rho(V|T,P) = \frac{1}{\sqrt{2\pi\sigma_V^2}} \exp\left[-\frac{(V-V_*)^2}{2\sigma_V^2}\right], \tag{A3}$$

where V_* and σ_V^2 are the mean and variance of the volume, respectively. We define $\langle(\cdots)\rangle_{T,P} = \int_0^\infty \mathrm{d}V\rho(V|T,P)(\cdots)$. Using this average, we can write $V_* = \langle V\rangle_{T,P}$ and $\sigma_V^2 = \langle(V - V_*)^2\rangle_{T,P}$.

2. Total entropy

The total entropy $S_{tot}(T, P)$ is obtained by a thermodynamic integration of the isobaric heat capacity from a reference temperature $T_{ref} = 1/\beta_{ref}$ to the target temperature $T = 1/\beta$,

$$\begin{aligned} S_{tot}(T,P) = S_{tot}(T_{ref},P) &- \frac{Nd}{2}(\ln\beta - \ln\beta_{ref}) + \beta U_*(T,P) \\ &- \beta_{ref}U_*(T_{ref},P) - \int_{\beta_{ref}}^{\beta} \mathrm{d}\beta' U_*(T',P) \\ &+ P(\beta V_*(T,P) - \beta_{ref}V_*(T_{ref},P)) \\ &- P\int_{\beta_{ref}}^{\beta} \mathrm{d}\beta' V_*(T',P), \end{aligned} \tag{A4}$$

where $U_*(T, P)$ is the mean potential energy and $V_*(T, P)$ is the mean volume; $U_*(T, P)$ and $V_*(T, P)$ are measured by constant pressure simulations. The entropy at the reference state is obtained by $S_{tot}(T_{ref}, P) = \langle S_{tot}(T_{ref}, V)\rangle_{T,P}$ using the NVT ensemble scheme.[44] This treatment for the reference state will be justified below.

3. Glass entropy

To get the glass entropy, we use the generalized Frenkel-Ladd method which relies on the NVT ensemble.[45] In general, one can smoothly connect NVT and NPT ensembles in terms of mean values. For example, thermodynamics guarantees that $S(T, P) = S(T, \langle V\rangle_{T,P})$. However, special attention should be paid if one uses the NVT ensemble scheme with trajectories generated by the NPT ensemble for finite system size.[113] A related issue is discussed in Ref. 114. Indeed, what we can compute is $\langle S(T, V)\rangle_{T,P}$. In general,

$$S(T,P) = \langle S(T,V)\rangle_{T,P} - \langle \ln\rho(V|T,P)\rangle_{T,P}. \tag{A5}$$

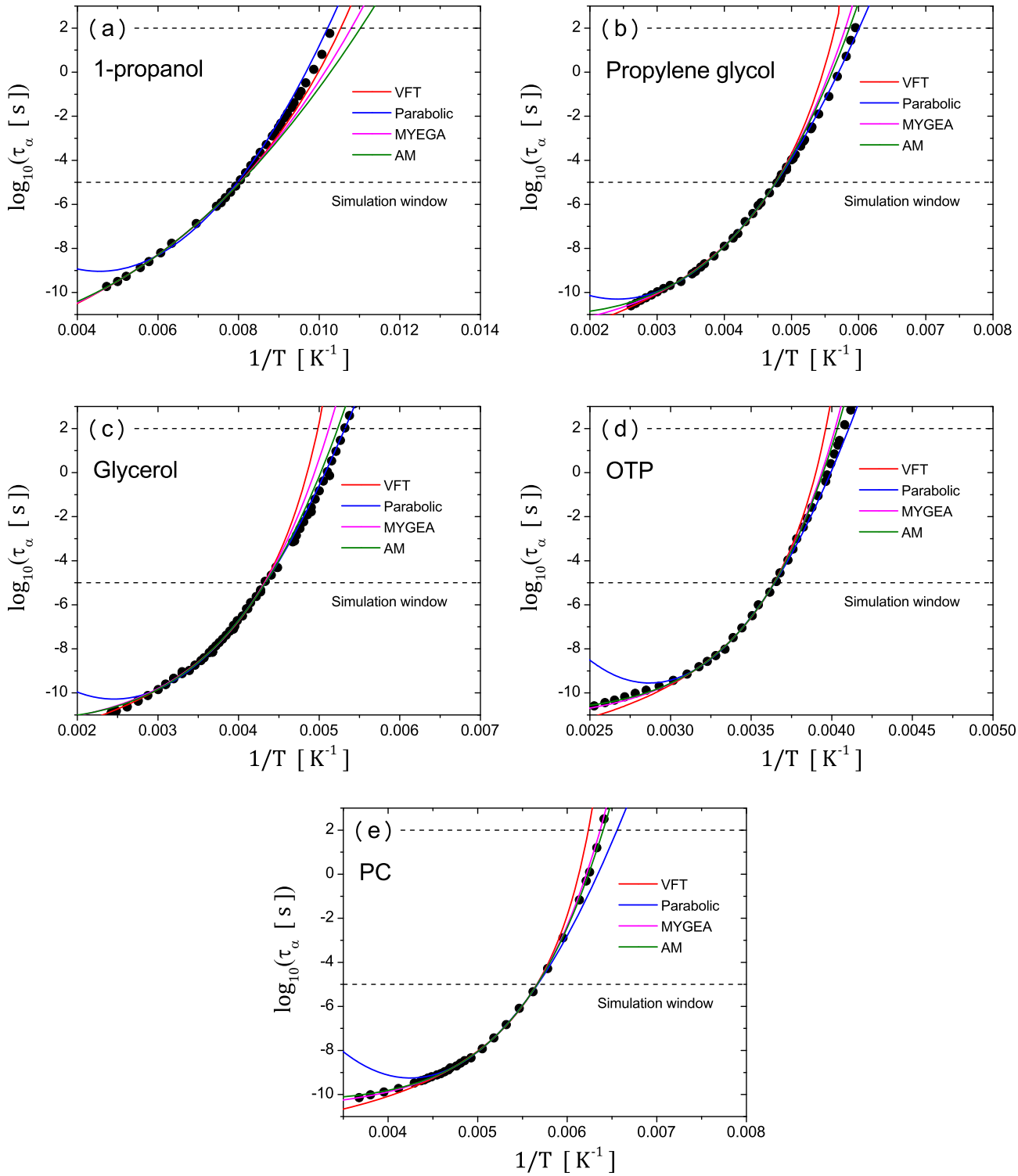

FIG. 8. Extrapolation from simulation time scale ($\tau_\alpha \leq 10^{-5}$ s) to experimental time scale for 1-propanol (a), propylene glycol (b), glycerol (c), OTP (d), and PC (e), whose kinetic fragility is equal to m = 35, 48, 53, 78, and 104, respectively. The values of m for 1-propanol, propylene glycol, and glycerol are comparable to the simulation models employed in this paper.

Therefore, we need to consider the second term in Eq. (A5) as a correction term. We can evaluate this term with Eq. (A3),

$$-\frac{1}{N}\langle \ln \rho(V|T,P)\rangle_{T,P} = \frac{1}{N}\ln\sqrt{2\pi e\sigma_V^2}. \tag{A6}$$

Since $\sigma_V^2 \sim N$, this term vanishes in the thermodynamic limit, as expected. Indeed, for $N = 1500$ systems, we get negligible values, $\frac{1}{N}\ln\sqrt{2\pi e\sigma_V^2} \simeq 0.0026$ and 0.0013 at $T_{\rm ref} = 7.0$ and $T = 0.37$, respectively. These values are small compared to the absolute value of $S_{\rm conf}/N \simeq 0.36$–$0.80$. Thus, we can safely use $S(T, P) = \langle S(T, V)\rangle_{T,P}$. Especially, we use the following equation, $S_{\rm glass}(T,P) = \langle S_{\rm glass}(T,V)\rangle_{T,P}$.

APPENDIX B: EXTRAPOLATION OF RELAXATION TIMES TOWARD T_g

Here, we test the validity of the extrapolation of relaxation time from the numerical to the experimental time scale using various fitting functions. We employ 1-propanol, propylene glycol, glycerol, OTP, and PC. Among these, 1-propanol, propylene glycol, and glycerol have kinetic fragility indexes similar to the simulation models.

Figure 8 shows various fits of the data performed over the simulation time window, $\tau_\alpha \le 10^{-5}$ s, and then extrapolated to lower temperatures down to T_g, where $\tau_\alpha = 100$ s. In the cases for 1-propanol, propylene glycol, glycerol, and OTP shown in Fig. 8, the parabolic law is the best functional form that predicts the actual data well over the experimental time window. All other functional forms, when fitted over the simulation time window, tend to deviate from the actual data at low temperatures. For the most fragile material, PC underestimates the actual data when the parabolic law is applied, whereas MYGEA and AM predict the data better. Notice that the uncertainty on the determination of T_g using the numerical time window and a parabolic fit is very small for the systems whose fragility is comparable to typical simulations models. This is the strategy we have used in previous numerical studies.[42–44]

REFERENCES

[1] G. Adam and J. H. Gibbs, "On the temperature dependence of cooperative relaxation properties in glass-forming liquids," J. Chem. Phys. **43**, 139 (1965).
[2] L. Berthier and G. Biroli, "Theoretical perspective on the glass transition and amorphous materials," Rev. Mod. Phys. **83**, 587 (2011).
[3] T. R. Kirkpatrick, D. Thirumalai, and P. G. Wolynes, "Scaling concepts for the dynamics of viscous liquids near an ideal glassy state," Phys. Rev. A **40**, 1045–1054 (1989).
[4] J.-P. Bouchaud and G. Biroli, "On the Adam-Gibbs-Kirkpatrick-Thirumalai-Wolynes scenario for the viscosity increase in glasses," J. Chem. Phys. **121**, 7347–7354 (2004).
[5] V. Lubchenko and P. G. Wolynes, "Theory of structural glasses and supercooled liquids," Annu. Rev. Phys. Chem. **58**, 235–266 (2007).
[6] G. Biroli and J. P. Bouchaud, "The random first-order transition theory of glasses: A critical assessment," in *Structural Glasses and Supercooled Liquids: Theory, Experiment and Applications*, edited by P. G. Wolynes and V. Lubchenko (Wiley & Sons, 2012); e-print arXiv:0912.2542.
[7] V. Lubchenko, "Theory of the structural glass transition: A pedagogical review," Adv. Phys. **64**, 283–443 (2015).
[8] P. Charbonneau, J. Kurchan, G. Parisi, P. Urbani, and F. Zamponi, "Glass and jamming transitions: From exact results to finite-dimensional descriptions," Annu. Rev. Condens. Matter Phys. **8**, 265–288 (2017).
[9] J. Dudowicz, K. F. Freed, and J. F. Douglas, "Generalized entropy theory of polymer glass formation," Adv. Chem. Phys. **137**, 125–222 (2008).
[10] C. A. Angell, "Entropy and fragility in supercooling liquids," J. Res. Natl. Inst. Stand. Technol. **102**, 171 (1997).
[11] R. Richert and C. A. Angell, "Dynamics of glass-forming liquids. V. On the link between molecular dynamics and configurational entropy," J. Chem. Phys. **108**, 9016–9026 (1998).
[12] S. Sastry, "The relationship between fragility, configurational entropy and the potential energy landscape of glass-forming liquids," Nature **409**, 164 (2001).
[13] J. C. Dyre, T. Hechsher, and K. Niss, "A brief critique of the Adam–Gibbs entropy model," J. Non-Cryst. Solids **355**, 624–627 (2009).
[14] F. Sciortino, W. Kob, and P. Tartaglia, "Inherent structure entropy of supercooled liquids," Phys. Rev. Lett. **83**, 3214–3217 (1999).
[15] S. Sastry, "Evaluation of the configurational entropy of a model liquid from computer simulations," J. Phys.: Condens. Matter **12**, 6515–6523 (2000).
[16] L. Berthier, M. Ozawa, and C. Scalliet, "Configurational entropy of glass-forming liquids," J. Chem. Phys. **150**, 160902 (2019).
[17] S. Mossa, E. La Nave, H. E. Stanley, C. Donati, F. Sciortino, and P. Tartaglia, "Dynamics and configurational entropy in the Lewis-Wahnström model for supercooled orthoterphenyl," Phys. Rev. E **65**, 041205 (2002).
[18] F. Sciortino, "Potential energy landscape description of supercooled liquids and glasses," J. Stat. Mech.: Theory Exp. **2005**, P05015.
[19] I. Saika-Voivod, P. H. Poole, and F. Sciortino, "Fragile-to-strong transition and polyamorphism in the energy landscape of liquid silica," Nature **412**, 514 (2001).
[20] L. Angelani, G. Foffi, F. Sciortino, and P. Tartaglia, "Diffusivity and configurational entropy maxima in short range attractive colloids," J. Phys.: Condens. Matter **17**, L113–L119 (2005).
[21] S. Sengupta, S. Karmakar, C. Dasgupta, and S. Sastry, "Adam-Gibbs relation for glass-forming liquids in two, three, and four dimensions," Phys. Rev. Lett. **109**, 095705 (2012).
[22] F. W. Starr, J. F. Douglas, and S. Sastry, "The relationship of dynamical heterogeneity to the Adam-Gibbs and random first-order transition theories of glass formation," J. Chem. Phys. **138**, 12A541 (2013).
[23] A. D. S. Parmar, S. Sengupta, and S. Sastry, "Length-scale dependence of the Stokes-Einstein and Adam-Gibbs relations in model glass formers," Phys. Rev. Lett. **119**, 056001 (2017).
[24] P. H. Handle and F. Sciortino, "The Adam–Gibbs relation and the TIP4P/2005 model of water," Mol. Phys. **116**, 3366–3371 (2018).
[25] W. Götze, *Complex Dynamics of Glass-Forming Liquids: A Mode-Coupling Theory* (Oxford University Press, Oxford, 2008), Vol. 143.
[26] J. H. Magill, "Physical properties of aromatic hydrocarbons. iii. A test of the Adam–Gibbs relaxation model for glass formers based on the heat-capacity data of 1, 3, 5-tri-α-naphthylbenzene," J. Chem. Phys. **47**, 2802–2807 (1967).
[27] S. Takahara, O. Yamamuro, and T. Matsuo, "Calorimetric study of 3-bromopentane: Correlation between structural relaxation time and configurational entropy," J. Phys. Chem. **99**, 9589–9592 (1995).
[28] K. L. Ngai, "Modification of the Adam–Gibbs model of glass transition for consistency with experimental data," J. Phys. Chem. B **103**, 5895–5902 (1999).
[29] C. Alba-Simionesco, "Salient properties of glassforming liquids close to the glass transition," C. R. Acad. Sci., Ser. IV: Phys., Astrophys. **2**, 203–216 (2001).
[30] C. M. Roland, S. Capaccioli, M. Lucchesi, and R. Casalini, "Adam–Gibbs model for the supercooled dynamics in the ortho-terphenyl ortho-phenylphenol mixture," J. Chem. Phys. **120**, 10640–10646 (2004).
[31] D. Cangialosi, A. Alegria, and J. Colmenero, "Relationship between dynamics and thermodynamics in glass-forming polymers," Europhys. Lett. **70**, 614 (2005).
[32] E. Masiewicz, A. Grzybowski, K. Grzybowska, S. Pawlus, J. Pionteck, and M. Paluch, "Adam-Gibbs model in the density scaling regime and its implications for the configurational entropy scaling," Sci. Rep. **5**, 13998 (2015).
[33] C. Cammarota, A. Cavagna, G. Gradenigo, T. Grigera, and P. Verrocchio, "Numerical determination of the exponents controlling the relationship between time, length, and temperature in glass-forming liquids," J. Chem. Phys. **131**, 194901 (2009).

[34]S. Karmakar, C. Dasgupta, and S. Sastry, "Growing length and time scales in glass-forming liquids," Proc. Natl. Acad. Sci. U. S. A. **106**, 3675–3679 (2009).
[35]G. M. Hocky, T. E. Markland, and D. R. Reichman, "Growing point-to-set length scale correlates with growing relaxation times in model supercooled liquids," Phys. Rev. Lett. **108**, 225506 (2012).
[36]R. Gutiérrez, S. Karmakar, Y. G. Pollack, and I. Procaccia, "The static lengthscale characterizing the glass transition at lower temperatures," Europhys. Lett. **111**, 56009 (2015).
[37]A. Cavagna, T. S. Grigera, and P. Verrocchio, "Dynamic relaxation of a liquid cavity under amorphous boundary conditions," J. Chem. Phys. **136**, 204502 (2012).
[38]S. Capaccioli, G. Ruocco, and F. Zamponi, "Dynamically correlated regions and configurational entropy in supercooled liquids," J. Phys. Chem. B **112**, 10652–10658 (2008).
[39]C. Brun, F. Ladieu, D. L'Hôte, G. Biroli, and J. P. Bouchaud, "Evidence of growing spatial correlations during the aging of glassy glycerol," Phys. Rev. Lett. **109**, 175702 (2012).
[40]L. Berthier, G. Biroli, J.-P. Bouchaud, L. Cipelletti, D. El Masri, D. L'Hôte, F. Ladieu, and M. Pierno, "Direct experimental evidence of a growing length scale accompanying the glass transition," Science **310**, 1797–1800 (2005).
[41]L. Berthier, D. Coslovich, A. Ninarello, and M. Ozawa, "Equilibrium sampling of hard spheres up to the jamming density and beyond," Phys. Rev. Lett. **116**, 238002 (2016).
[42]A. Ninarello, L. Berthier, and D. Coslovich, "Models and algorithms for the next generation of glass transition studies," Phys. Rev. X **7**, 021039 (2017).
[43]L. Berthier, P. Charbonneau, A. Ninarello, M. Ozawa, and S. Yaida, "Zero-temperature glass transition in two dimensions," Nat. Commun. **10**, 1508 (2019).
[44]L. Berthier, P. Charbonneau, D. Coslovich, A. Ninarello, M. Ozawa, and S. Yaida, "Configurational entropy measurements in extremely supercooled liquids that break the glass ceiling," Proc. Natl. Acad. Sci. U. S. A. **114**, 11356–11361 (2017).
[45]M. Ozawa, G. Parisi, and L. Berthier, "Configurational entropy of polydisperse supercooled liquids," J. Chem. Phys. **149**, 154501 (2018).
[46]S. Tatsumi, S. Aso, and O. Yamamuro, "Thermodynamic study of simple molecular glasses: Universal features in their heat capacity and the size of the cooperatively rearranging regions," Phys. Rev. Lett. **109**, 045701 (2012).
[47]L. Berthier, E. Flenner, C. J. Fullerton, C. Scalliet, and M. Singh, "Efficient swap algorithms for molecular dynamics simulations of equilibrium supercooled liquids," J. Stat. Mech. **2019**, 064004; preprint arXiv:1811.12837.
[48]L. Berthier and T. A. Witten, "Glass transition of dense fluids of hard and compressible spheres," Phys. Rev. E **80**, 021502 (2009).
[49]A. Banerjee, S. Sengupta, S. Sastry, and S. M. Bhattacharyya, "Role of structure and entropy in determining differences in dynamics for glass formers with different interaction potentials," Phys. Rev. Lett. **113**, 225701 (2014).
[50]G. Biroli, J. P. Bouchaud, A. Cavagna, T. S. Grigera, and P. Verrocchio, "Thermodynamic signature of growing amorphous order in glass-forming liquids," Nat. Phys. **4**, 771–775 (2008).
[51]L. Berthier, P. Charbonneau, and S. Yaida, "Efficient measurement of point-to-set correlations and overlap fluctuations in glass-forming liquids," J. Chem. Phys. **144**, 024501 (2016).
[52]L. Berthier and W. Kob, "The Monte Carlo dynamics of a binary Lennard-Jones glass-forming mixture," J. Phys.: Condens. Matter **19**, 205130 (2007).
[53]E. Flenner and G. Szamel, "Fundamental differences between glassy dynamics in two and three dimensions," Nat. Commun. **6**, 7392 (2015).
[54]F. Stickel, E. W. Fischer, and R. Richert, "Dynamics of glass-forming liquids. I. Temperature-derivative analysis of dielectric relaxation data," J. Chem. Phys. **102**, 6251–6257 (1995).
[55]M. E. Blodgett, T. Egami, Z. Nussinov, and K. F. Kelton, "Proposal for universality in the viscosity of metallic liquids," Sci. Rep. **5**, 13837 (2015).
[56]Y. S. Elmatad, D. Chandler, and J. P. Garrahan, "Corresponding states of structural glass formers. II," J. Phys. Chem. B **114**, 17113–17119 (2010).
[57]J. C. Mauro, Y. Yue, A. J. Ellison, P. K. Gupta, and D. C. Allan, "Viscosity of glass-forming liquids," Proc. Natl. Acad. Sci. U. S. A. **106**, 19780–19784 (2009).
[58]I. Avramov and A. Milchev, "Effect of disorder on diffusion and viscosity in condensed systems," J. Non-Cryst. Solids **104**, 253–260 (1988).
[59]D. Coslovich, M. Ozawa, and K. Walter, "Dynamic and thermodynamic crossover scenarios in the KoB-Andersen mixture: Insights from multi-CPU and multi-GPU simulations," Eur. Phys. J. E **41**, 62 (2018).
[60]V. N. Novikov and A. P. Sokolov, "Universality of the dynamic crossover in glass-forming liquids: A 'magic' relaxation time," Phys. Rev. E **67**, 031507 (2003).
[61]C. P. Royall, F. Turci, S. Tatsumi, J. Russo, and J. Robinson, "The race to the bottom: Approaching the ideal glass?," J. Phys.: Condens. Matter **30**, 363001 (2018).
[62]S. Takahara, O. Yamamuro, and H. Suga, "Heat capacities and glass transitions of 1-propanol and 3-methylpentane under pressure. New evidence for the entropy theory," J. Non-Cryst. Solids **171**, 259–270 (1994).
[63]A. Yoshimori and T. Odagaki, "Configurational entropy and heat capacity in supercooled liquids," J. Phys. Soc. Jpn. **80**, 064601 (2011).
[64]H. L. Smith, C. W. Li, A. Hoff, G. R. Garrett, D. S. Kim, F. C. Yang, M. S. Lucas, T. Swan-Wood, J. Y. Y. Lin, M. B. Stone *et al.*, "Separating the configurational and vibrational entropy contributions in metallic glasses," Nat. Phys. **13**, 900 (2017).
[65]K. Takeda, O. Yamamuro, I. Tsukushi, T. Matsuo, and H. Suga, "Calorimetric study of ethylene glycol and 1, 3-propanediol: Configurational entropy in supercooled polyalcohols," J. Mol. Struct. **479**, 227–235 (1999).
[66]O. Haida, H. Suga, and S. Seki, "Calorimetric study of the glassy state XII. Plural glass-transition phenomena of ethanol," J. Chem. Thermodyn. **9**, 1133–1148 (1977).
[67]G. E. Gibson and W. F. Giauque, "The third law of thermodynamics. Evidence from the specific heats of glycerol that the entropy of a glass exceeds that of a crystal at the absolute zero," J. Am. Chem. Soc. **45**, 93–104 (1923).
[68]M. S. Beasley, C. Bishop, B. J. Kasting, and M. D. Ediger, "Vapor-deposited ethylbenzene glasses approach 'ideal glass' density," J. Phys. Chem. Lett. **10**, 4069 (2019).
[69]Z. Chen and R. Richert, "Dynamics of glass-forming liquids. XV. Dynamical features of molecular liquids that form ultra-stable glasses by vapor deposition," J. Chem. Phys. **135**, 124515 (2011).
[70]A. J. Barlow, J. Lamb, and A. J. Matheson, "Viscous behaviour of supercooled liquids," Proc. R. Soc. London, Ser. A **292**, 322–342 (1966).
[71]F. D. Rossini, *Selected Values of Physical and Thermodynamic Properties of Hydrocarbons and Related Compounds: Comprising the Tables of the American Petroleum Institute Research Project 44 Extant as of December 31, 1952* (American Petroleum Institute, 1953), Vol. 44.
[72]U. Schneider, P. Lunkenheimer, R. Brand, and A. Loidl, "Dielectric and far-infrared spectroscopy of glycerol," J. Non-Cryst. Solids **235**, 173–179 (1998).
[73]P. Lunkenheimer, U. Schneider, R. Brand, and A. Loid, "Glassy dynamics," Contemp. Phys. **41**, 15–36 (2000).
[74]P. Lunkenheimer, R. Wehn, U. Schneider, and A. Loidl, "Glassy aging dynamics," Phys. Rev. Lett. **95**, 055702 (2005).
[75]B. Schmidtke, N. Petzold, R. Kahlau, M. Hofmann, and E. A. Rössler, "From boiling point to glass transition temperature: Transport coefficients in molecular liquids follow three-parameter scaling," Phys. Rev. E **86**, 041507 (2012).
[76]C. Hansen, F. Stickel, T. Berger, R. Richert, and E. W. Fischer, "Dynamics of glass-forming liquids. III. Comparing the dielectric α-and β-relaxation of 1-propanol and o-terphenyl," J. Chem. Phys. **107**, 1086–1093 (1997).
[77]P. Sillrén, A. Matic, M. Karlsson, M. Koza, M. Maccarini, P. Fouquet, M. Götz, T. Bauer, R. Gulich, P. Lunkenheimer *et al.*, "Liquid 1-propanol studied by neutron scattering, near-infrared, and dielectric spectroscopy," J. Chem. Phys. **140**, 124501 (2014).
[78]U. Schneider, P. Lunkenheimer, R. Brand, and A. Loidl, "Broadband dielectric spectroscopy on glass-forming propylene carbonate," Phys. Rev. E **59**, 6924–6936 (1999).
[79]F. Stickel, E. W. Fischer, and R. Richert, "Dynamics of glass-forming liquids. II. Detailed comparison of dielectric relaxation, DC-conductivity, and viscosity data," J. Chem. Phys. **104**, 2043–2055 (1996).
[80]J. G. Berberian and R. H. Cole, "Approach to glassy behavior of dielectric relaxation in 3-bromopentane from 298 to 107 k," J. Chem. Phys. **84**, 6921–6927 (1986).

[81] S. Tatsumi and O. Yamamuro (unpublished).
[82] R. Brand, P. Lunkenheimer, U. Schneider, and A. Loidl, "Excess wing in the dielectric loss of glass-forming ethanol: A relaxation process," Phys. Rev. B **62**, 8878–8883 (2000).
[83] *Understanding Molecular Simulation*, 2nd ed., edited by D. Frenkel and B. Smit (Academic Press, San Diego, 2002).
[84] S. Franz and G. Parisi, "Phase diagram of coupled glassy systems: A mean-field study," Phys. Rev. Lett. **79**, 2486–2489 (1997).
[85] L. Berthier and D. Coslovich, "Novel approach to numerical measurements of the configurational entropy in supercooled liquids," Proc. Natl. Acad. Sci. U. S. A. **111**, 11668–11672 (2014).
[86] S. Franz, "First steps of a nucleation theory in disordered systems," J. Stat. Mech.: Theory Exp. **2005**, P04001.
[87] L. Berthier, P. Charbonneau, and J. Kundu, "Bypassing sluggishness: Swap algorithm and glassiness in high dimensions," Phys. Rev. E **99**, 031301 (2019).
[88] V. Lubchenko and P. Rabochiy, "On the mechanism of activated transport in glassy liquids," J. Phys. Chem. B **118**, 13744–13759 (2014).
[89] G. Tarjus, "An overview of the theories of the glass transition," in *Dynamical Heterogeneities and Glasses*, edited by L. Berthier, G. Biroli, J.-P. Bouchaud, L. Cipelletti, and W. van Saarloos (Oxford University Press, 2011); e-print arXiv:1010.2938.
[90] C. Cammarota, A. Cavagna, G. Gradenigo, T. S. Grigera, and P. Verrocchio, "Evidence for a spinodal limit of amorphous excitations in glassy systems," J. Stat. Mech.: Theory Exp. **2009**, L12002.
[91] D. Ganapathi, K. H. Nagamanasa, A. K. Sood, and R. Ganapathy, ""Measurements of growing surface tension of amorphous–amorphous interfaces on approaching the colloidal glass transition," Nat. Commun. **9**, 397 (2018).
[92] Y. Z. Chua, A. R. Young-Gonzales, R. Richert, M. D. Ediger, and C. Schick, "Dynamics of supercooled liquid and plastic crystalline ethanol: Dielectric relaxation and ac nanocalorimetry distinguish structural α-and Debye relaxation processes," J. Chem. Phys. **147**, 014502 (2017).
[93] M. Goldstein, "Viscous liquids and the glass transition. V. Sources of the excess specific heat of the liquid," J. Chem. Phys. **64**, 4767–4774 (1976).
[94] O. Yamamuro, I. Tsukushi, A. Lindqvist, S. Takahara, M. Ishikawa, and T. Matsuo, "Calorimetric study of glassy and liquid toluene and ethylbenzene:? Thermodynamic approach to spatial heterogeneity in glass-forming molecular liquids," J. Phys. Chem. B **102**, 1605–1609 (1998).
[95] G. P. Johari, "Contributions to the entropy of a glass and liquid, and the dielectric relaxation time," J. Chem. Phys. **112**, 7518–7523 (2000).
[96] L.-M. Martinez and C. A. Angell, "A thermodynamic connection to the fragility of glass-forming liquids," Nature **410**, 663 (2001).
[97] C. A. Angell and S. Borick, "Specific heats c_p, c_v, c_{conf} conf and energy landscapes of glassforming liquids," J. Non-Cryst. Solids **307**, 393 (2002).
[98] R. Alvarez-Donado and A. Antonelli, "Vibrational and configurational entropy separation in bulk metallic glasses: A thermodynamic approach," preprint arXiv:1907.02611 (2019).
[99] D. Han, D. Wei, J. Yang, H.-L. Li, M.-Q. Jiang, Y.-J. Wang, L.-H. Dai, and A. Zaccone, "Structural atomistic mechanism for the glass transition entropic scenario," preprint arXiv:1907.03695 (2019).
[100] M. Ozawa and L. Berthier, "Does the configurational entropy of polydisperse particles exist?," J. Chem. Phys. **146**, 014502 (2017).
[101] D. S. Fisher and D. A. Huse, "Nonequilibrium dynamics of spin glasses," Phys. Rev. B **38**, 373 (1988).
[102] I. Balog and G. Tarjus, "Activated dynamic scaling in the random-field Ising model: A nonperturbative functional renormalization group approach," Phys. Rev. B **91**, 214201 (2015).
[103] H. Tanaka, "Relation between thermodynamics and kinetics of glass-forming liquids," Phys. Rev. Lett. **90**, 055701 (2003).
[104] T. Hecksher, A. I. Nielsen, N. B. Olsen, and J. C. Dyre, "Little evidence for dynamic divergences in ultraviscous molecular liquids," Nat. Phys. **4**, 737 (2008).
[105] G. Tarjus, S. A. Kivelson, Z. Nussinov, and P. Viot, "The frustration-based approach of supercooled liquids and the glass transition: A review and critical assessment," J. Phys.: Condens. Matter **17**, R1143–R1182 (2005).
[106] P. Rabochiy, P. G. Wolynes, and V. Lubchenko, "Microscopically based calculations of the free energy barrier and dynamic length scale in supercooled liquids: The comparative role of configurational entropy and elasticity," J. Phys. Chem. B **117**, 15204–15219 (2013).
[107] M. Wyart and M. E. Cates, "Does a growing static length scale control the glass transition?," Phys. Rev. Lett. **119**, 195501 (2017).
[108] J. C. Dyre, "Colloquium: The glass transition and elastic models of glass-forming liquids," Rev. Mod. Phys. **78**, 953–972 (2006).
[109] H. Tanaka, "Bond orientational order in liquids: Towards a unified description of water-like anomalies, liquid-liquid transition, glass transition, and crystallization," Eur. Phys. J. E **35**, 113 (2012).
[110] H. Ikeda, F. Zamponi, and A. Ikeda, "Mean field theory of the swap Monte Carlo algorithm," J. Chem. Phys. **147**, 234506 (2017).
[111] S. Yaida, L. Berthier, P. Charbonneau, and G. Tarjus, "Point-to-set lengths, local structure, and glassiness," Phys. Rev. E **94**, 032605 (2016).
[112] D. Chandler and J. P. Garrahan, "Dynamics on the way to forming glass: Bubbles in space-time," Annu. Rev. Phys. Chem. **61**, 191–217 (2010).
[113] J. L. Lebowitz, J. K. Percus, and L. Verlet, "Ensemble dependence of fluctuations with application to machine computations," Phys. Rev. **153**, 250–254 (1967).
[114] B. Cheng and M. Ceriotti, "Computing the absolute Gibbs free energy in atomistic simulations: Applications to defects in solids," Phys. Rev. B **97**, 054102 (2018).